Effect of Different Chromium Additions on the Microstructure and Mechanical Properties of Multipass Weld Joint of Duplex Stainless Steel

DONG HOON KANG and HAE WOO LEE

The correlation between the mechanical properties and ferrite volume fraction (approximately 40, 50, and 60 Ferrite Number [FN]) in duplex stainless steel weld metals were investigated by changing the Cr content in filler wires with a flux-cored arc-welding (FCAW) process. The interpass temperature was thoroughly maintained under a maximum of 423 K (150 °C), and the heat input was also sustained at a level under 15 KJ/cm in order to minimize defects. The microstructure examination demonstrated that the δ-ferrite volume fraction in the deposited metals increased as the Cr/Ni equivalent ratio increased, and consequently, chromium nitride (Cr_2N) precipitation was prone to occur in the ferrite domains due to low solubility of nitrogen in this phase. Thus, more dislocations are pinned by the precipitates, thereby lowering the mobility of the dislocations. Not only can this lead to the strength improvement, but also it can accentuate embrittlement of the weld metal at subzero temperature. Additionally, the solid-solution strengthening by an increase of Cr and Mo content in austenite phase depending on the reduction of austenite proportion also made an impact on the increase of the tensile and yield strength. On the other hand, the impact test (at 293 K, 223 K, and 173 K [20 °C, –50 °C, and –100 °C]) showed that the specimen containing about 40 to 50 FN had the best result. The absorbed energy of about 40 to 50 J sufficiently satisfied the requirements for industrial applications at 223 K (–50 °C), while the ductile-to-brittle transition behavior exhibited in weldment containing 60 FN. As the test temperature decreased under 223 K (–50 °C), a narrow and deep dimple was transformed into a wide and shallow dimple, and a significant portion of the fracture surface was occupied by a flat cleavage facet with river patterns.

I. INTRODUCTION

DUPLEX stainless steels (DSS) are widely used in many environments and operating conditions, such as in the marine, chemical, petrochemical, nuclear, fertilizer, and food industries, because of their superior performance in comparison to traditional austenitic stainless steel. DSSs have higher strengths than austenitic stainless steels, higher toughness levels than ferritic stainless steels, good weldability, and high resistance to stress corrosion cracking. These good properties depend on the two-phase microstructure that consists of approximately equal volume fractions of γ-austenite and δ-ferrite phases.[1–4] Since the development of first-generation DSSs in the 1930s, continuing research effort have been exerted to improve both mechanical and corrosion properties, particularly by controlling alloying elements of Cr, Mo, N, W, *etc.*[5–8] Currently, however, most of the research on DSS has been performed on the wrought products, and only a limited number of studies has been reported on the weld products of DSSs, despite their

significance in the industry. Large industrial applications of duplex stainless steels utilize welding as a manufacturing process. Therefore, it is also very important to maintain an optimum phase balance in weld metal after welding. However, welding of DSS results in a disturbed phase balance, and this problem is more significant in flux-cored arc welding (FCAW) processes because of their low heat input and very fast cooling rates.[9] The resultant weld metals contain higher ferrite levels and have been reported to have inferior properties.[10] In order to restore the toughness of welded connections, weld filler materials are usually overalloyed with 2 to 4 pct more Ni than in the base material.[11] During recent years, the authors studied the mechanical behaviors of DSS welds with varying alloying elements and reported that the mechanical properties were strongly influenced by the change in the shape and volume fraction of austenitic phase with different amounts of additions. For example, Muthupandi *et al.*[12] examined the effect of nickel and nitrogen addition on the microstructure and mechanical properties of DSS weld metals, and they found that not only does the introduction of Ni or N not influence the hardness of resultant weld metals, but also these elements improve the impact toughness substantially at subzero temperature. Park and Lee[13] studied the effect of nitrogen and heat treatment on the microstructure

DONG HOON KANG, Master Degree, and HAE WOO LEE, Professor, are with the Department of Materials Science and Engineering, Dong-A University, Saha-gu, Busan 604-714, Republic of Korea. Contact e-mails: hwlee@dau.ac.kr; cartoon83@nate.com

and tensile properties of 25Cr-7Ni-1.5Mo-3W-xN DSS castings, and consequently, it was revealed that the increase of ferrite volume fraction decreases the tensile strength and the elongation, and it increases the yield strength of the casting linearly. Some authors[14] have reported that manganese additions increased the toughness and the ultimate tensile strength of stainless steel, but it had little effect on the yield strength. Cr is a strong ferrite-stabilizing element and is known to improve the resistance to corrosion by the formation of a stable passive film on the structure of the stainless steel.[15,16] Despite the beneficial effect of Cr in stainless steel, the effect of Cr on the mechanical behaviors of DSS welds has not been well established.

The aim of this current study was, therefore, to examine the effect of the addition Cr on the microstructure and mechanical properties of the weld fusion zone. Specifically, the investigation focused on a comparison of the low-temperature impact behavior of the DSS weld with different δ/γ ratios, based on the SEM micrographic and fractographic observations.

II. EXPERIMENTAL DETAILS

A. Test Panel/Filler Wire Preparation and Welding Process

The test panels, which were 300 mm long × 100 mm wide × 12 mm thick, were butt welded in four layers with a root gap opening of 3 mm and a total V-groove angle of 34 deg 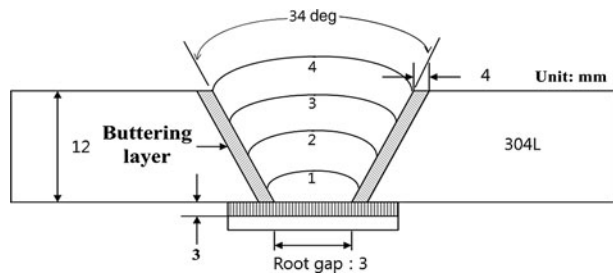under a strong restraint condition to avoid thermal distortion, and this was performed in the plat position by a FCAW process using three newly designed types of 1.2-mm-diameter filler wires, which were fabricated based on the AWS 2209TO (1)-1/4 electrode by modifying the Cr contents in the flux to obtain three different volume fractions. Each groove and backing material was buttered up to 4 mm with the same filler wires in this study to minimize the dilution between the AISI304L austenitic SS and DSS weld metal, so the buttering layer was not considered in the investigation. A schematic diagram of the weldment and the welding parameters is shown in Figure 1 and Table I, respectively. The welded specimens were sectioned as shown in Figure 2 indicating the location of the different test specimens, and then the correlation of weld metal microstructure with mechanical properties was investigated.

B. Equivalent Formula

The Cr/Ni equivalent ratio was computed to the WRC-1992 formula.[17]

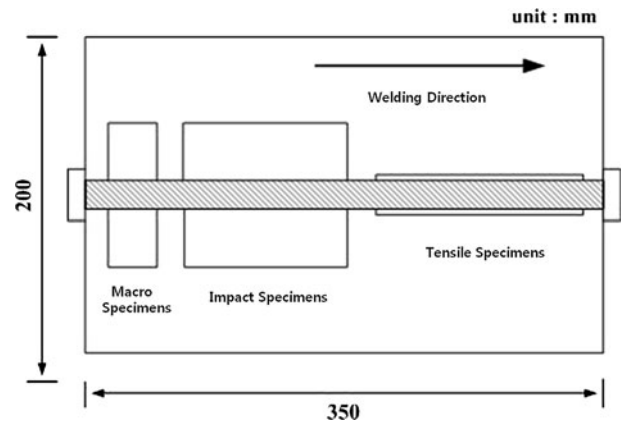$$Cr_{eq} = Cr + Mo + 0.7Nb$$

$$Ni_{eq} = Ni + 35C + 20N + 0.25Cu$$

Fig. 1—Schematic diagram of the weldment.

Fig. 2—Location of test specimens.

Table I. Welding Parameters

Test No.	No. of Layers	Current (A)	Voltage (V)	Interpass Temperature (°C)	Travel Speed (cm/min)	Heat Input (KJ/cm)
No. 1	1	140	28	19	26	9.0
	2	170	29	77	28	10.2
	3	180	30	106	34	9.4
	4	180	30	127	21	15.3
No. 2	1	140	28	22	30	7.6
	2	170	29	72	29	10.0
	3	180	30	92	32	9.9
	4	180	30	120	21	15.5
No. 3	1	140	28	15	27	8.6
	2	170	29	45	28	10.3
	3	180	30	77	30	10.8
	4	180	30	123	21	15.0

Shielding gas/flow rate: CO_2 (100 pct), 20 mL/min, polarity: DCRP(+) electrode extension (mm): 15 to 20.

Table II. Chemical Composition of the Weld Metal (Weight Percent)

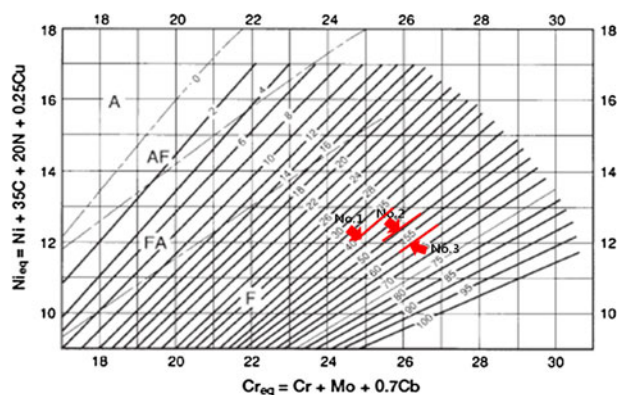| As-Weld Metals	C	N	Si	Mn	P	S	Cr	Ni	Mo	Cu	Nb	Cr_{eq}	Ni_{eq}	Cr_{eq}/Ni_{eq}
No. 1	0.032	0.112	0.81	0.62	0.024	0.008	21.30	8.71	3.41	0.07	0.003	24.72	12.08	2.02
No. 2	0.029	0.114	0.82	0.59	0.025	0.008	22.03	8.73	3.28	0.07	0.003	25.31	12.03	2.10
No. 3	0.030	0.115	0.9	0.61	0.024	0.007	22.82	8.70	3.37	0.07	0.004	26.19	12.06	2.18

Fig. 3—FNs of specimens on the WRC-1992 diagram.

The chemical analysis for the three welds, which were named as No. 1, No. 2, and No. 3, respectively, was performed using a hybrid optic spectrometer (Metal-LAB75/80J, GNR, srl, Rome, Italy), and the results are shown in Table II.

C. Ferrite Number (FN) Prediction

Ferrite measurements were also used to produce quantitative relationships between alloy composition and ferrite volume fraction, and the results were then plotted on the WRC-1992 weld constitution diagram as shown in Figure 3. Good agreement was shown between the solidification mode of primary ferrite alloys and those predicted by the WRC-1992 diagram. A ferrite-scope (MP30E-S, Fischer Scientific, Schwerte, Germany) was used in the nondestructive evaluation to observe the ferrite content on the weldments in terms of the FN, and the details are listed in Table III.

D. Microstructure/Fracture Analysis

The specimens were ground with 2000-grit emery paper and polished successively with 3-μm diamond pastes, rinsed with water, subjected to ultrasonic cleaning, and dried in air. Then they were immersed in boiling Murakami's reagent (10 g K3Fe(CN)6, 10 g KOH, and 100 mL H_2O heated to 373 K (100 °C) for 1 hour) in order to measure its volume fraction.[18] For observation of the microstructure and fractograph, scanning electron microscopy with an energy dispersive spectroscopy (SEM-EDS) (JSM-6700f; JEOL Ltd., Tokyo, Japan) detector was used.

E. Impact/Tensile/Hardness Test

The specimens for the Charpy-V impact test were machined (subsize type A – V notch, dimensions:

Table III. FN of Weld Metals

Specimen	Face	Center	Root	Average	WRC-1992
		Ferrite Scope			
No. 1	50	40	47	45	42
No. 2	60	50	56	55	51
No. 3	75	60	70	68	62

7.5 × 10 × 55 mm) as shown in Figure 4; they were tested at room temperature, 223 K and 173 K (–50 °C and –100 °C) according to ASTM E23-05. The data were then converted to a standard size (10 by 10 mm) according to the A 370-05 acceptance criteria table. The strength was measured using a universal testing machine (AG-25TG; Shimadzu, Tokyo, Japan). Round-bar-type tensile test specimens (ASTM E8-04) were prepared from the fully deposited metal in a direction parallel to the welding direction. The hardness tests were performed on a Vickers hardness tester FM700 applying a maximum load of 1 kg for dwell times of at least 10 seconds. More detailed studies of the hardness alternation were performed using Vickers HV0.05 method. Thirty measurements of each phase in weld metal at a depth of 7 mm from the surface, and the results were averaged for subsequent analysis.

III. RESULTS AND DISCUSSION

A. Macrostructure/Microstructure

Figure 5 shows a good external FCAW macrostructure (12 mm, four pass). The geometry of the weld joint was fully penetrated and deposited. Additionally, no visible porosity or defect was observed on the weldment. As shown in Figure 6, the transformation sequence for duplex stainless steel is as follows[2]:

$$L \rightarrow L + F \rightarrow F \rightarrow F + A \quad [F \text{ mode}]$$
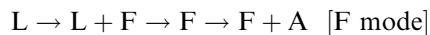
The nature of the ferrite-to-austenite transformation in dependent on both the chemical composition and its total thermal history.[10,19] Welds, however, and their heat-affected zones (HAZs) are rapidly cooled from temperatures near the ferrite solvus, so there is a tendency for appreciably more ferrite in the weld metal and HAZ of a duplex stainless steel than there is in the base metal. It is considered that, therefore, the chemical composition can be even more crucial factor to maintain the ferrite-austenite balance in the weld metal. For this reason, each of the specimens was manufactured by controlling the
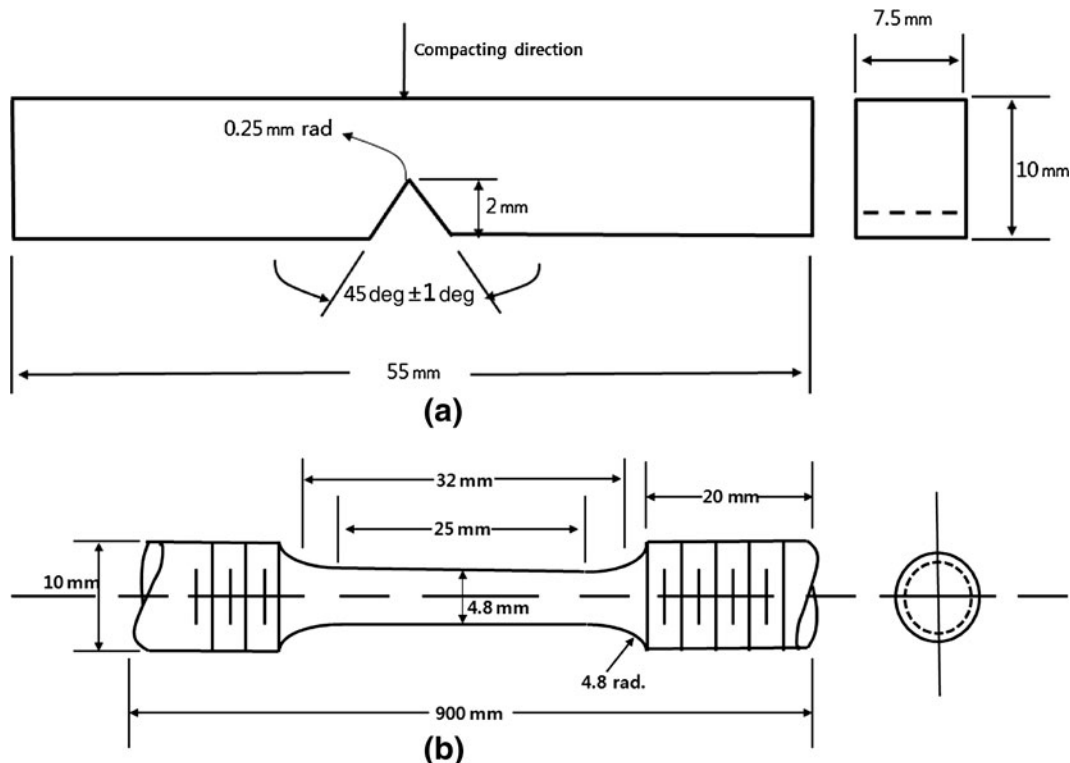
Fig. 4—Dimensions of tensile and impact specimens. (*a*) Charpy (simple-beam) subsize (Type A, V-notch) impact test specimens. (*b*) Round tension test specimen (threaded end).

Fig. 5—Macrography of the four-pass weld joint.

Fig. 6—Relationship of solidification type to the pseudobinary phase diagram.

Cr/Ni equivalent ratio while maintaining the heat input constantly, for the purpose of changing the ferrite-austenite volume fraction of the weldment.[20,21]

In the weld metal, ferrite solidification involves epitaxial growth from the parent material at the fusion boundary. The initial dendrite growth is oriented in relation to the thermal gradient, and this produces a columnar ferritic structure. The initial nucleation and growth process of the austenite phase occurs intergranularly; then, it completes the coverage of the ferrite grain boundaries. Additional austenite may form as Widmanstätten side plates off the grain boundary austenite or it may form intragranularly withi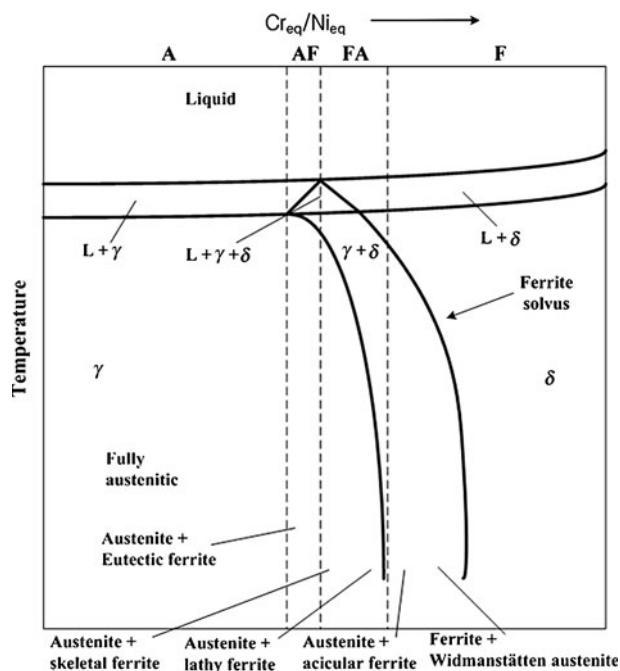n the ferrite grains.[10] As can be seen in Figure 7, in the optical microstructure of the weld metal, the dark part represents ferrite while the light part represents austenite. The microstructure of Figure 7(a) is composed of about 40 FN, Figure 7(b) is composed of about 50 FN, and Figure 7(c) is composed of about 60 FN by
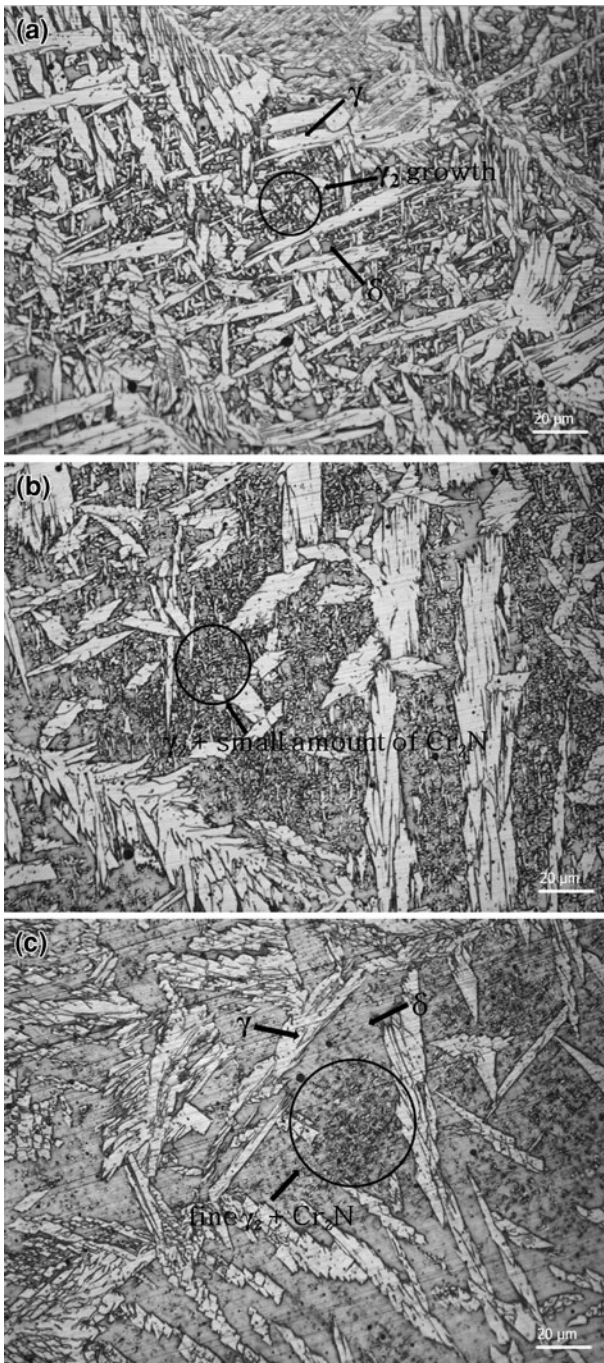
Fig. 7—Optical micrograph of the weld metal: dark etched regions (ferrite), light etched region (austenite). (*a*) No. 1, 42 FN; (*b*) No. 2, 51 FN; and (*c*) No. 3, 62 FN.

Fig. 8—X-ray diffraction results of specimen No. 3 (as-weld).

reference of WRC-1992 formula. In addition to the changes in the austenite morphologies present in the fusion zone, some precipitates could also be observed within the ferrite grains.

Figure 8 indicates the X-ray diffraction results of specimen No. 3. These figures show only peaks corresponding to the reflections of ferrite and austenite crystalline planes; no secondary phase was identified by this technique. The fact that the X-ray test did not detect other precipitates in the material's microstructure does
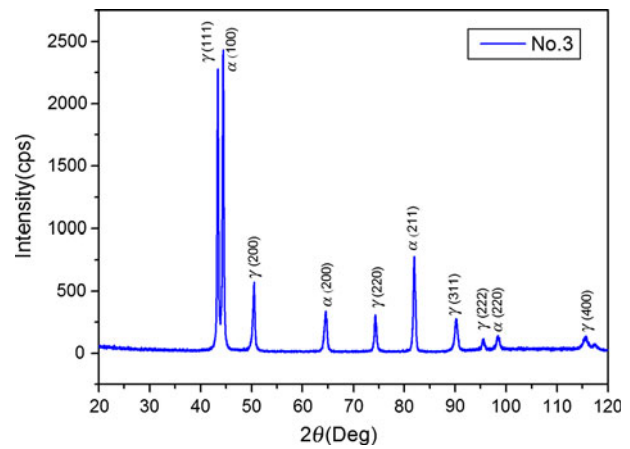
not mean they do not exist. They may be present in concentrations of less than 3 pct, which is the lowest detection limit, or there are only atom clusters in the initial stages of formation of a precipitate coherent with the matrix. According to Ramirez *et al.*,[22] these precipitates are believed to be Cr_2N and secondary austenite (γ_2). The formation of these Cr_2N within the ferritized microstructure is aided by this rapid cooling from temperatures above 1373 K (1100 °C), which creates a supersaturated solid solution, primarily of Cr and N, in the interior of the ferrite grains, resulting in a competition between chromium nitride and austenite precipitation. These chromium nitrides precipitate from the ferrite by nucleation and growth, following a kinetic "C" curve. Nucleation takes place at dislocation, inclusions, and grain boundaries.[23] This chromium nitride precipitation has been shown to severely impair the corrosion resistance and the toughness of the DSSs.[23–25] When the material in this metastable condition is reheated, as in multipass welding, the most apparent changes in the microstructure are the dissolution of the intragranular nitrides and the precipitation of secondary austenite (γ_2). According to these studies,[26,27] the nitrogen liberated by the nitride dissolution, in the temperature range of 1273 K to 1473 K (1000 °C to 1200 °C), facilitates the γ_2 nucleation. It is also well known that the γ_2 precipitation improves the toughness of the material.[26] Figure 9 presents an SEM micrograph of specimen No. 3 (as-weld). Needle-like Cr_2N precipitates (arrow marks) were found in the ferrite grains or at the α/α subgrain boundaries. These particles had an average thickness of 0.05 to 0.2 μm and a length of 0.3 to 1 μm.

B. Hardness Test

The hardness values were recorded on a transverse section of the deposited weld metal at a depth of 7 mm from the surface using a Vickers hardness testing machine, and the results are presented in graphical form as shown in Figure 10(a). Comparing the three specimens, No. 3 had the highest hardness value, followed in order by specimens No. 2 and No. 1. Figure 10(b) shows the variation of hardness measured
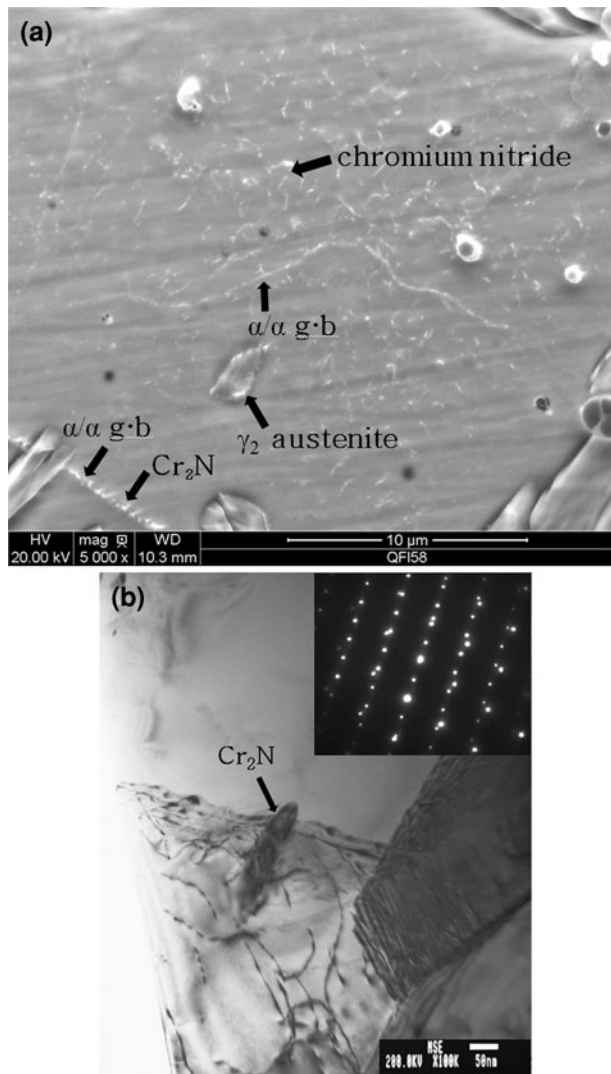
Fig. 9—Nitride colony in the interior of a ferrite grain in specimen No. 3: (a) secondary electron SEM image, (b) TEM micrographs of Cr$_2$N precipitates: bright-field image and selected-area diffraction pattern $\left(z = [111]_\alpha // [01\bar{1}0]_{\text{Cr}_2\text{N}} \right)$.

for ferrite and austenite phase in each specimens. The hardness in both phases increased proportionally within similar value with the increase of Cr content in the filler wire. For example, the indentation size on both the ferrite and austenite phases in the specimen No. 2 are nearly the same as the hardness of the both phases are in the same range, i.e., 270 to 285 HV0.05 (Figure 10(c)). This means that differences in the ferrite–austenite ratio have little effect on the hardness of the material.

In general, it has been reported that the ferrite and austenite phases do not differ much in composition because the substitutional elements do not have time to partition significantly during DSS welding and with interstitial nitrogen; only the austenite amount varies but not its hardness.[10] But the findings show a regular difference between the chemical composition of δ and γ phase in spite of the fusion zone. Table IV shows the average chemical composition of major alloying elements in the ferrite and austenite phase analyzed by
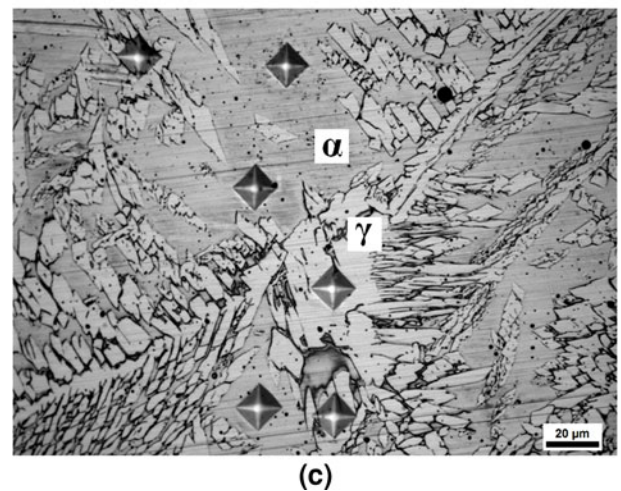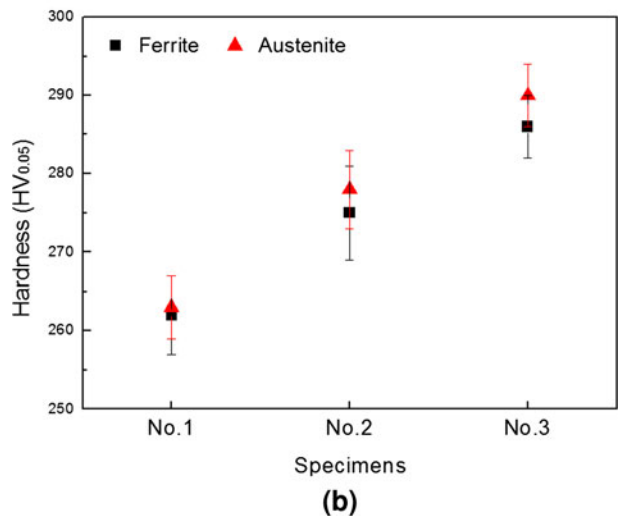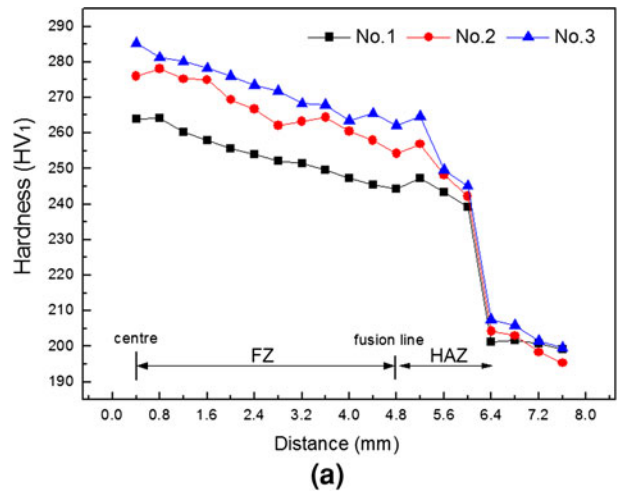

Fig. 10—Hardness testing results. (a) Hardness traverses along 7-mm distance from top surface in FCAW process. (b) Variation of hardness measured for ferrite and austenite phase in each specimens. (c) Vickers microhardness indentation on ferrite and austenite phase of specimen No. 2.

SEM-EDS. The δ-ferrite phase contains a few more Cr and Mo, while the Ni and N are partitioned preferentially to the austenite phase. Although the ferrite volume

Table IV. Average Major Alloying Element Content of Ferrite and Austenite Phases

	Phase	Volume	Cr	Ni	Mo	N	P	Cu
No. 1	Ferrite	35 pct	23.49	8.24	3.99	0.08	0.11	0.05
	Austenite	65 pct	20.11	9.81	2.81	0.27	0.03	0.38
No. 2	Ferrite	43 pct	23.70	7.91	3.68	0.06	0.12	0.04
	Austenite	57 pct	21.53	10.02	2.98	0.29	0.04	0.42
No. 3	Ferrite	51 pct	23.81	7.72	3.42	0.06	0.13	0.05
	Austenite	49 pct	21.87	10.31	3.07	0.30	0.03	0.45

fraction is high in specimen No. 3, it should be noted that Cr content slightly increased in δ-ferrite due to an increase of Cr content in the filler wire, whereas Cr and Mo are incremented sequentially for each γ-austenite depending on the decrease of the austenite volume fraction. Also, there is no observable change in nitrogen. It is, therefore, also estimated that substitutional effect by Cr and Mo is more influential than interstitial solid-solution strengthening by nitrogen in austenite phase.

On the other hand, the hardness of ferrite phase has risen slightly despite the reduction in Mo content. The possibility of chromium nitride formation during welding has been indicated in several studies.[28,29] If the ferrite content is high, such as in the weld metal and HAZ under rapid cooling conditions, then an intense nitride precipitation reaction occurs upon cooling since the solubility limit of the ferrite is exceeded and the nitrogen has insufficient time to partition to the austenite. The presence of chromium nitride particles within a ferrite grain can be clearly seen as shown in Figure 9. Since sigma (σ) and chi (χ) phases were not observed in the weld metal, the higher hardness value of ferrite phase can be attributed to Cr_2N precipitation. In a word, it can be deduced that the presence of Cr_2N play an important role as a pinning site limiting the movement of mobile dislocation. The frequently observed accumulations and alignment of chromium nitrides at ferrite grain boundaries correspond to the high dislocation density of those boundaries and can be explained through the diffusion impediment of nitrogen at these dislocations during rapid cooling. The partial annealing zone (PAZ) adjacent to the base metal and the base metal ruled out profile analysis due to the buttering layer diluted with the AISI 304L.

C. Tensile Behavior

The tensile properties obtained after the tensile tests for each specimen are shown in Figure 11 and compared with those of SAF 2207. Each data point represents the average of at least three test results. The results show that as the chromium in AWS 2209 filler wire increases, there is increase in both yield strength (YS) and ultimate tensile strength (UTS) as compared with those of SAF 2207. The YS has increased by 31 pct and 43 pct and UTS has also increased by 9 pct and 14 pct. The elongation of the weld metal normally has a lower value than that of the base metal.[30] However, the elongation of No. 1 and No. 2 can reach a level that is about 25 pct of the value of the base metal due to an increased 9 wt pct Ni content in filler wire, whereas that of No. 3 reduced by increasing the ferrite volume fraction. It is obvious that the
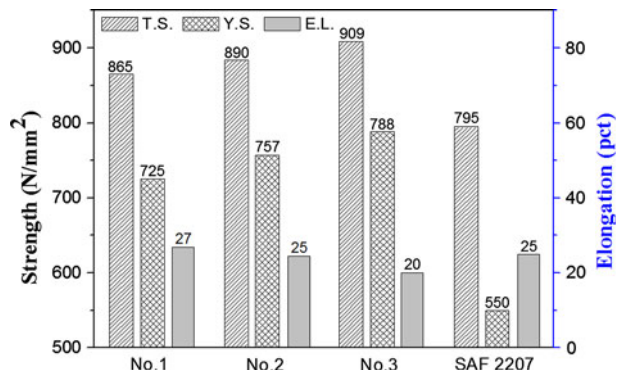

Fig. 11—The result of mechanical strength test.

variation of phase ratio by Cr content leads to significant change in the tensile properties of DSS. Li et al.[8] noted that the increase in γ-phase as a result of increase in Mn and N enhances the ultimate tensile strength and ductility. Park and Lee[13] also reported that an increase of ferrite volume fraction decreases the tensile strength, and the elongation and increases the yield strength of the DSS castings almost linearly with decreasing N content. It is well known that in DSS, most of the nitrogen is dissolved in austenite, which makes austenite the stronger phase due to interstitial solid-solution strengthening by nitrogen.[31] In this study, on the other hand, it is interesting to note that both the YS and UTS were increased along with increasing the volume fraction of ferrite. As mentioned above, this result was caused by three crucial factors: (1) solid-solution strengthening by an increase of Cr and Mo content in austenite phase, (2) stacking of mobile dislocation by the precipitates in ferrite phase, (3) the difference of the Peierls stress between the body-centered cubic (bcc; ferrite) and face-centered cubic (fcc; austenite) materials.[32] This is further discussed in Section III–D.

Figure 12 illustrates the damage process: cleavage crack nucleation in the ferrite and subsequent growth in the austenite that creates cavities. Final rupture is produced by the coalescence of these cavities. Although rupture is initiated by cleavage, the overall fracture mechanism remains ductile.

D. Impact Toughness

The impact toughness values estimated by Charpy impact testing both at 293 K, 223 K, and 173 K (20 °C, –50 °C, and –100 °C) for the FCAW metals are shown in Figure 13. As a result, the absorbed energy of
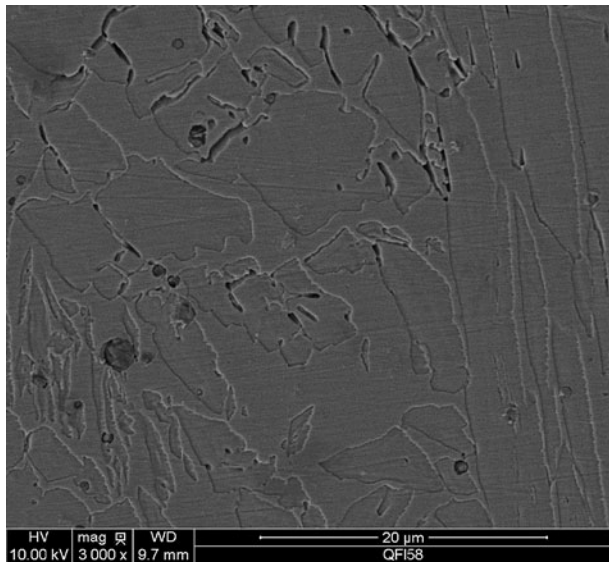
Fig. 12—Surface crack nucleation in the ferrite and subsequent void growth during a tensile test.
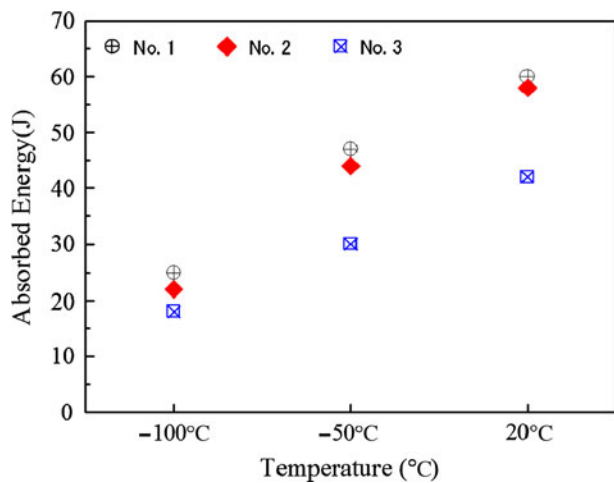

Fig. 13—Results of Charpy V-notch impact tests for weld metal in FCAW process.

specimen No. 1 was the highest, followed in order by specimens No. 2 and No. 3. The toughness values of No. 1 (42 FN) and No. 2 (51 FN) show that although differences exist in the ferrite content among the weld metals, they all exhibit nearly the same toughness until 223 K (–50 °C) impact tests, and these weld metals sufficiently meet the subzero impact toughness requirements for industrial applications, whereas No. 3 (61FN) showed a significant drop. On the other hand, the results obtained from the test conducted at 173 K (–100 °C) showed that the ferrite–austenite ratio has a significant role to play in declining the low-temperature toughness.

It is well known that the influence of the ferrite content on the absorbed energy was reported to be negligible up to about 50 pct to 60 pct (60-85 FN) ferrite,[10] whereas there is a clear negative influence at higher ferrite levels. Furthermore, there may be a negative effect due to ferrite contents below 35 pct

(38 FN), apparently due to a change in solidification mode causing segregation and precipitation of intermetallic phase.[33] But these results (Figure 13) mean that weld metals must be maintained below 61 FN (50 pct) in order to restore toughness, although the filler wire with 2 to 4 pct more Ni than in the base material is used. The ductile-to-brittle transition temperature (DBTT) was normally determined at half the value of the total impact energy against the test temperature. Then, the values of DBTT are probably expected to be existed just below 223 K (–50 °C).

At subzero temperature, welds typically exhibit higher strength and lower toughness than their base metal counterparts. Chan[34] reported that the inferior weld metals toughness is associated with high nonmetallic inclusion and delta ferrite content, as well as higher strength level, and the δ-ferrite phase undergoes a ductile-to-brittle transition at or below 223 K (–50 °C). On the other hand, according to Lee et al.,[35] the austenite stainless steel weld metal fracture surface displayed ductile dimple rupture features at room temperature and even at 77 K (–196 °C). It can then be concluded that the austenite matrix has restricted the cleavage fracture mechanism that could have been formed around the deformed delta ferrite phase. In conclusion, the observed ductile-to-brittle transition behavior of the duplex stainless steel weld metals can be associated with the high ferrite proportion in their microstructure.

Since ferrite is of a bcc structure, its yield strength (which is a function of temperature) increases as the temperature is lowered due to an increased lattice friction stress and pinning of mobile dislocations with interstitial atoms. On the other hand, the cleavage fracture stress of ferrite is not a function of temperature and is only varied by microstructural parameters as grain size and dislocation density.[36] Additionally, it also may be explained with the Peierls stress, which was studied with regard to movement of the dislocation by temperature variation. The critical feature of the Peierls stress is that the yield strength is closely connected with the temperature; that is, the Peierls stress dramatically increases from the slow-down of the dislocation as the temperature decreased. The yield strength of the material increases as a result. This means a decrease of the absorbed energy at a lower temperature due to an inverse relationship between the yield strength and the toughness in the material.[37–39] According to Kacar,[40] at room temperature, the cleavage fracture stress of ferrite is much higher than its yield strength, and consequently, plastic deformation prevails and ductile behavior is verified. As temperature decreases, and at a certain low temperatures, the yield strength of ferrite becomes higher than its cleavage fracture stress. At this stage, a transition from ductile fracture through plastic deformation to brittle fracture by cleavage takes place. Since the austenite phase of the duplex stainless steel is of an fcc structure, neither of its yield nor fracture stress would be a function of temperature.[41,42] A possible additional reason is that the ferrite matrix was highly modulated, and all the dislocations were heavily jogged such that no straight dislocations can be observed. Besides, there were Cr_2N precipitates situated in the matrix or dislocation lines. This evidence suggested that

as the ferrite phase increases, more dislocations are pinned by the precipitates on the dislocation and the modulated matrix, thereby lowering the mobility of the dislocations. This pinning behavior is expected to lead to the embrittlement of the weld metals.

E. Fractographic Observation

Figure 14 shows detailed fracture morphologies as obtained under an SEM of the fracture surfaces from Charpy impact specimens varied with ferrite number. In the as-welded condition, the three specimens showed the similar tendency for fracture morphologies at three different temperatures (293 K, 223 K, and 173 K [20 °C, –50 °C, and –100 °C]), respectively. Figure 14(a) exhibits a ductile fracture mechanism characterized by a linked series of the structure that was composed of deep, narrow, and equiaxed dimples. A mixed mode of ductile and brittle fracture was observed after a 223 K (–50 °C) impact test (Figure 14(b)). The fracture appearance reveals dimples along with the occasional area of quasi-cleavage. As for the rest, the continuous dimple link snapped due to the existence of sparse quasi-cleavage areas. On the other hand, a significant portion of the fracture surface was occupied by a flat cleavage facet that had river patterns (as shown in Figure 14(c)), suggesting that the brittle fracture mechanism has become dominant. The whole appearance of the dimple assumed the form of a shallow, stretched, and quantal shape.[43] Notably, river pattern areas coexist with small shallow dimples, which could be caused by the fracture of secondary austenite, and the tearing edges existed amidst the dimple rupture, which resulted in the break off of a stream of dimples such that the ligaments of austenite are sheared between the cleavage planes.[44]

Using an energy-dispersive X-ray analyzer equipped in the scanning electron microscope, a quantitative determination of chemistry was carried out on both cleavage of quasi-cleavage facets and dimple zones, respectively. The result of over 20 repeated tests were averaged to achieve 23.9 wt pct Cr and 7.7 wt pct Ni contents on the cleavage or quasi-cleavage facets, whereas the composition of average 20.3 wt pct Cr and 10.02 wt pct Ni was obtained on the dimple zone, for the No. 2 specimen. These results revealed that cleavage or quasi-cleavage occurred in the ferrite phase, whereas a ductile fracture with microvoid coalescence occurred in the austenitic phase. Viewed with respect to the overall phenomenon, such as above, the parameter that could contribute to the deformation mechanism of duplex stainless steel weldments, particularly at a subzero temperatures, is predicted to result from the amount of δ-ferrite phase contained in the microstructures. And it is also apparent that a drastic drop in toughness is connected with the embrittlement and cleavage of δ-ferrite.[45]

IV. CONCLUSIONS

The effect of the ferrite volume fraction by changing chromium content of filler wire on the microstructure
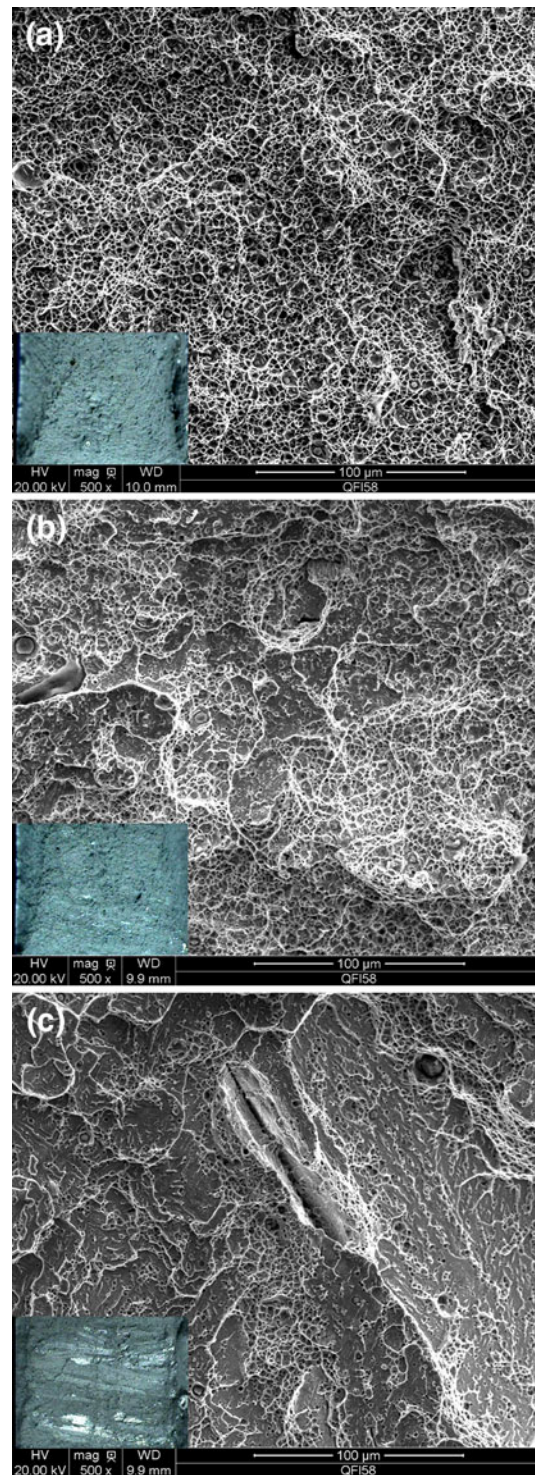

Fig. 14—SEM micrograph of the fracture surfaces of No. 3 specimen: (a) 293 K (20 °C), (b) 223 K (–50 °C), and (c) 173 K (–100 °C).

and mechanical properties of DSS weld metals were investigated. The study results can be summarized as follows:

1. The delta ferrite increased as the addition of Cr in the deposited metals increased, and consequently, chromium nitride (Cr_2N) precipitation was prone to

occur in the ferrite domains due to low solubility of nitrogen in this phase. Thus, more dislocations are pinned by the precipitates, thereby lowering the mobility of the dislocations. This leads not only to the strength improvement but also to embrittlement of the weld metal at subzero temperatures.

2. The frequently observed accumulations and alignment of chromium nitrides at ferrite subgrain boundaries correspond to the high dislocation density of those boundaries and can be explained through the diffusion impediment of nitrogen at these dislocations during rapid cooling.

3. The hardness of austenite phase was largely increased by substitutional effect by Cr and Mo rather than interstitial solid-solution strengthening by nitrogen, as the volume fraction of austenite decreased. That of the ferrite phase has risen linearly despite the reduction in Mo content, on the other hand, due to the precipitation hardening of Cr_2N. This phenomenon is also affecting the strength properties of DSS weld metals.

4. The absorbed energy of about 40 to 50 FN sufficiently satisfied the requirements (34 J at 253 K [–20 °C]) for industrial applications at 223 K (–50 °C), while the ductile-to-brittle transition behavior exhibited in weldment containing 60 FN. As the test temperature decreased less than 223 K (–50 °C), a narrow and deep dimple was transformed into a wide and shallow dimple. A significant portion of the fracture surface was occupied by a flat cleavage facet with river patterns.

ACKNOWLEDGMENT

REFERENCES

1. I. Varol and W.A. Baeslack, III: *Mater. Charact.*, 1997, vol. 39, pp. 553–73.
2. J.C. Lippold and D.J. Kotecki: *Welding Metallurgy and Weldability of Stainless Steels*, 1st ed., Hoboken, NJ, 2005, pp. 230–34.
3. H. Ericksson and S. Bernhardsson: *Corros. Sci.*, 1991, vol. 47, pp. 719–25.
4. J. Oredsson and S. Bernhardsson: *Mater. Perf.*, 1983, vol. 22, pp. 35–42.
5. J.I. Son, S.S. Kim, J.H. Lee, and B.H. Choi: *Metall. Mater. Trans. A*, 2003, vol. 34A, pp. 1617–25.
6. Y.H. Jang, S.S. Kim, and J.H. Lee: *Mater. Sci. Eng. A*, 2005, vol. 396, pp. 302–10.
7. S.B. Kim, K.W. Paik, and Y.K. Kim: *Mater. Sci. Eng. A*, 1998, vol. 247, pp. 67–74.
8. J. Li, Y. Xu, X. Xiao, J. Zhao, L. Jiang, and J. Hu: *Mater. Sci. Eng. A*, 2009, vol. 527, pp. 245–51.
9. S. Kou: *Welding Metallurgy*, 2nd ed., Wiley, Hoboken, NJ, 2003, pp. 3–29.
10. R.N Gunn: *Duplex Stainless Steel*, Woodhead Publishing Ltd., Abington, VA, 1997, pp. 110–19.
11. J.R. Davis: *Stainless Steels (ASM Specialty Handbook)*, ASM International, Materials Park, OH, 1994.
12. V. Muthupandi, P. Bala Srinivasan, V. Shankar, S.K. Seshadri, and S. Sundaresan: *Mater. Lett.*, 2005, vol. 59, pp. 2305–09.
13. Y.H. Park and Z.H. Lee: *Mater. Sci. Eng. A*, 2001, vol. 297, pp. 78–84.
14. M. Kemp, A. Van Bennekom, and F.P.A. Robinson: *Mater. Sci. Eng. A*, 1995, vol. 199, pp. 183–94.
15. J. Sakai, I. Matsushima, Y. Kamemura, M. Tanimura, and T. Osuka: *Duplex Stainless Steels*, R.A. Lula, ed., ASM International, Materials Park, OH, 1983, pp. 211–31.
16. R.A. Perren, T. Suter, C. Solenthaler, G. Gullo, P.J. Uggowitzer, H. Böhni, and M.O. Speidel: *Corros. Sci.*, 2001, vol. 43, pp. 727–45.
17. D.J. Kotecki and T.A. Sievert: *Weld. J.*, 1992, vol. 71, pp. 171–78.
18. D.E. Nelson and W.A. Baeslack, III: *Mater. Charact.*, 1997, vol. 39, pp. 467–77.
19. R. Badji, M. Bouabdallah, B. Bacroix, C. Kahloun, B. Belkessa, and H. Maza: *Mater. Charact.*, 2008, vol. 59, pp. 447–53.
20. D.J. Lee, J.C. Byun, J.H. Sung, and H.W. Lee: *Mater. Sci. Eng. A*, 2009, vol. 513, p. 154.
21. Y.H. Kim, D.J. Lee, J.C. Byun, K.H. Jung, J.I. Kim, H.J. Lee, Y.T. Shin, S.H. Kim, and H.W. Lee: *Mater. Des.*, 2011, vol. 32, pp. 330–36.
22. A.J. Ramirez, J.C. Lippold, and S.D. Brandi: *Metall. Mater. Trans. A*, 2003, vol. 34A, pp. 1575–97.
23. S.D. Brandi and A.J. Ramirez: *Duplex Stainless Steels '97*, Proc. Conf., KCI, Maastricht, the Netherlands, 1997, pp. 405–10.
24. V.S. Moura, L.D. Limda, J.M. Pardal, A.Y. Kina, R.R.A. Corte, and S.S.M. Tavares: *Mater. Charact.*, 2008, vol. 59, pp. 1127–32.
25. B. Deng, Z. Wang, Y. Jiang, T. Sun, J. Xu, and J. Li: *Corros. Sci.*, 2009, vol. 51, pp. 2969–75.
26. J.C. Lippold and A.M. Al-Rumaih: *Duplex Stainless Steels '97*, Proc. Conf., KCI, Maastricht, the Netherlands, 1997, pp. 405–10.
27. S.D. Brandi, J.C. Lippold, and W. Lin: *Duplex Stainless Steels '97*, Proc. Conf., KCI, Maastricht, the Netherlands, 1997, pp. 411–18.
28. T. Ogawa and T. Koseki: *Weld. J.*, 1989, vol. 68, pp. 181–91.
29. T.G. Gooch: *ASM Conference Proc. on Duplex Stainless Steels*, 1982, pp. 573–602.
30. J.D. Kordatos, G. Fourlaris, and G. Papadimitiou: *Scripta Mater.*, 2001, vol. 44, pp. 401–08.
31. J.W. Simmons: *Mater. Sci. Eng. A*, 1996, vol. 207, p. 159.
32. F.R.N. Nabarro: *Mater. Sci. Eng. A*, 1989, vol. 113, pp. 315–26.
33. S. Pak and L. Karlsson: *Scand. J. Metall.*, 1990, vol. 19, pp. 19–23.
34. J.W. Chan: *Adv. Cryog. Eng.*, 1992, vol. 55, pp. 34–38.
35. D.J. Lee, J.C. Byun, J.H. Sung, and H.W. Lee: *Mater. Sci. Eng. A*, 2009, vols. 513–514, pp. 154–59.
36. G. Han, S. Fukuyama, and K. Yokogawa: *Mater. Sci. Technol.*, 1999, vol. 15, pp. 905–09.
37. R. Peierls: *Proc. Phys. Soc.*, 1940, vol. 52, pp. 34–37.
38. G. Schoeck: *Mater. Sci. Eng. A*, 2005, vol. 400, pp. 7–17.
39. B. Deng, Z. Wang, Y. Jiang, T. Sun, J. Xu, and J. Li: *Corros. Sci.*, 2009, vol. 51, pp. 2969–75.
40. R. Kacar: *Mater. Des.*, 2004, vol. 25, pp. 1–9.
41. R. Kacar and M. Acarer: *Mater. Sci. Eng. A*, 2003, vol. 363, p. 290.
42. H. Sieurin and R. Sandstom: *Eng. Fract. Mech.*, 2006, vol. 73, p. 377.
43. Ceramics Metals and Information Center: *SEM/TEM Fractography Handbook*, Metals and Ceramics Information Center, Huntington, CA, 1975.
44. S. Bonnet, J. Bourgoin, J. Champredonde, D. Guttmann, and M. Guttmann: *Mater. Sci. Technol.*, 1990, vol. 6, pp. 221–29.
45. K. Chandra, R. Singhal, V. Kain, and V.S. Raja: *Mater. Sci. Eng. A*, 2010, vol. 527, pp. 3904–12.